Supplemental Appendix

Conformational changes in Arp2/3 complex induced by ATP, WASp-VCA and actin filaments

Sofia Espinoza-Sanchez[1,2], Lauren Ann Metskas[1,2,3], Steven Z. Chou[4], Elizabeth Rhoades[5] and Thomas D. Pollard[1,2,4,6]

[1]Department of Molecular Biophysics and Biochemistry, Yale University, New Haven, CT 06520
[2]Program in Physical and Engineering Biology, Yale University, New Haven, CT 06520
[3]Department of Biology and Biological Engineering, California Institute of Technology, Pasadena, CA 91125
[4]Department of Molecular, Cellular and Developmental Biology, Yale University, New Haven, CT 06520
[5]Department of Chemistry, University of Pennsylvania, Philadelphia, PA 19104
[6]Department of Cell Biology, Yale University, New Haven, CT 06520

www.pnas.org/cgi/doi/10.1073/pnas.1717574115

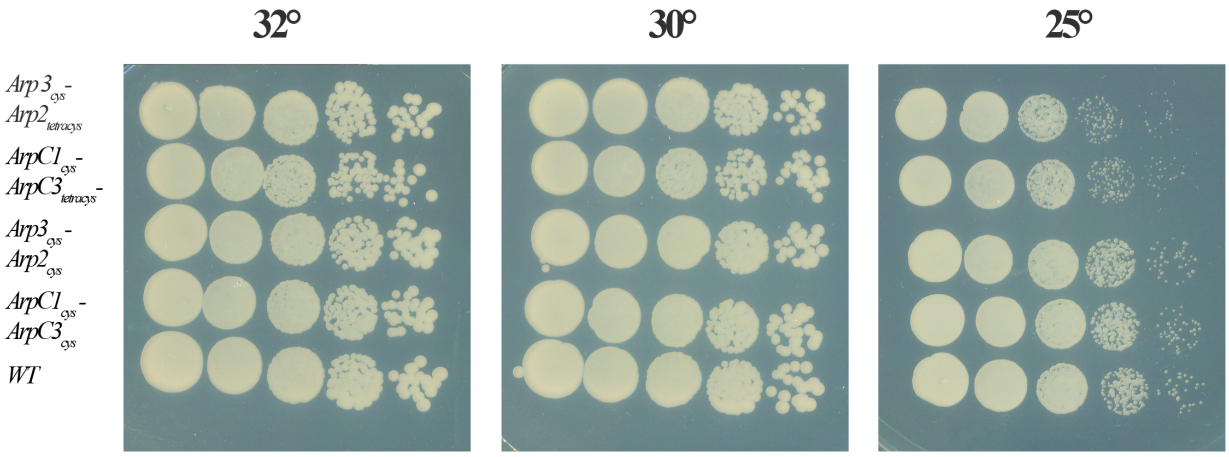

Figure S1. Growth of 10-fold dilutions of five yeast strains at 32°C, 30°C and 25°C on YE5S agar plates for 48 h.

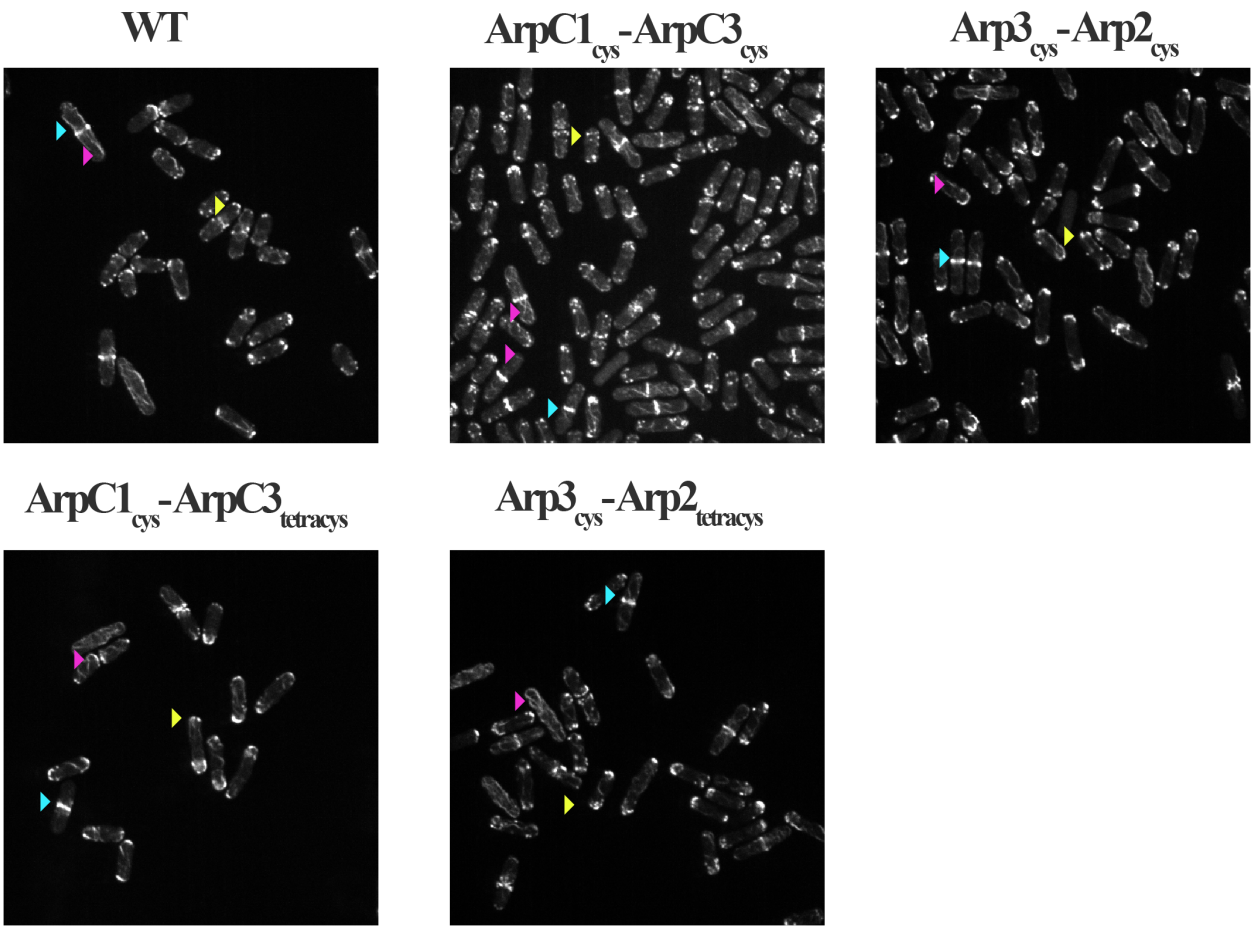

Figure S2. Confocal fluorescence micrographs of wild-type and mutant yeast strains stained with BODIPY-phalloidin to visualize actin filaments. All of the strains all had contractile rings (light blue arrowheads), endocytic actin patches (yellow arrowheads) and actin filament cables (magenta arrowheads). Cells were grown to OD_{600} = 0.6, fixed with 5% formaldehyde in TEM buffer (0.1M Tris-HCl pH 7.4, 1 mM EGTA, 1 mM $MgCl_2$), washed three times with TEM for 1 min each, permeabilized with 1% Triton X-100 in TEM for 5 min and washed with TEM buffer before treatment with 8 μM BODIPY-phalloidin in TEM buffer for 10 min. Cells were mounted on 25% gelatin pads for microscopy.

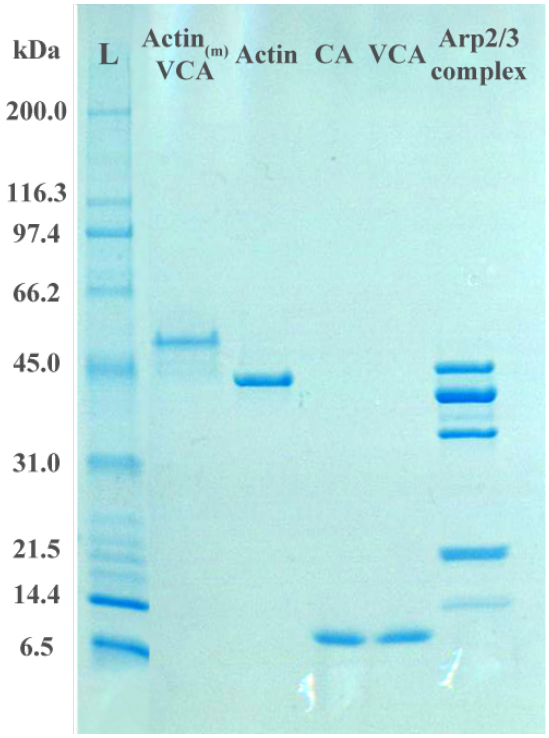

Figure S3. SDS-polyacrylamide gel electrophoresis of purified proteins stained with Coomassie Blue. Lane 1, Ladder of standard proteins; 2, actin-VCA; 3, actin; 4, Wsp1p-CA; 5, Wsp1p-VCA; 6, Arp2/3 complex.

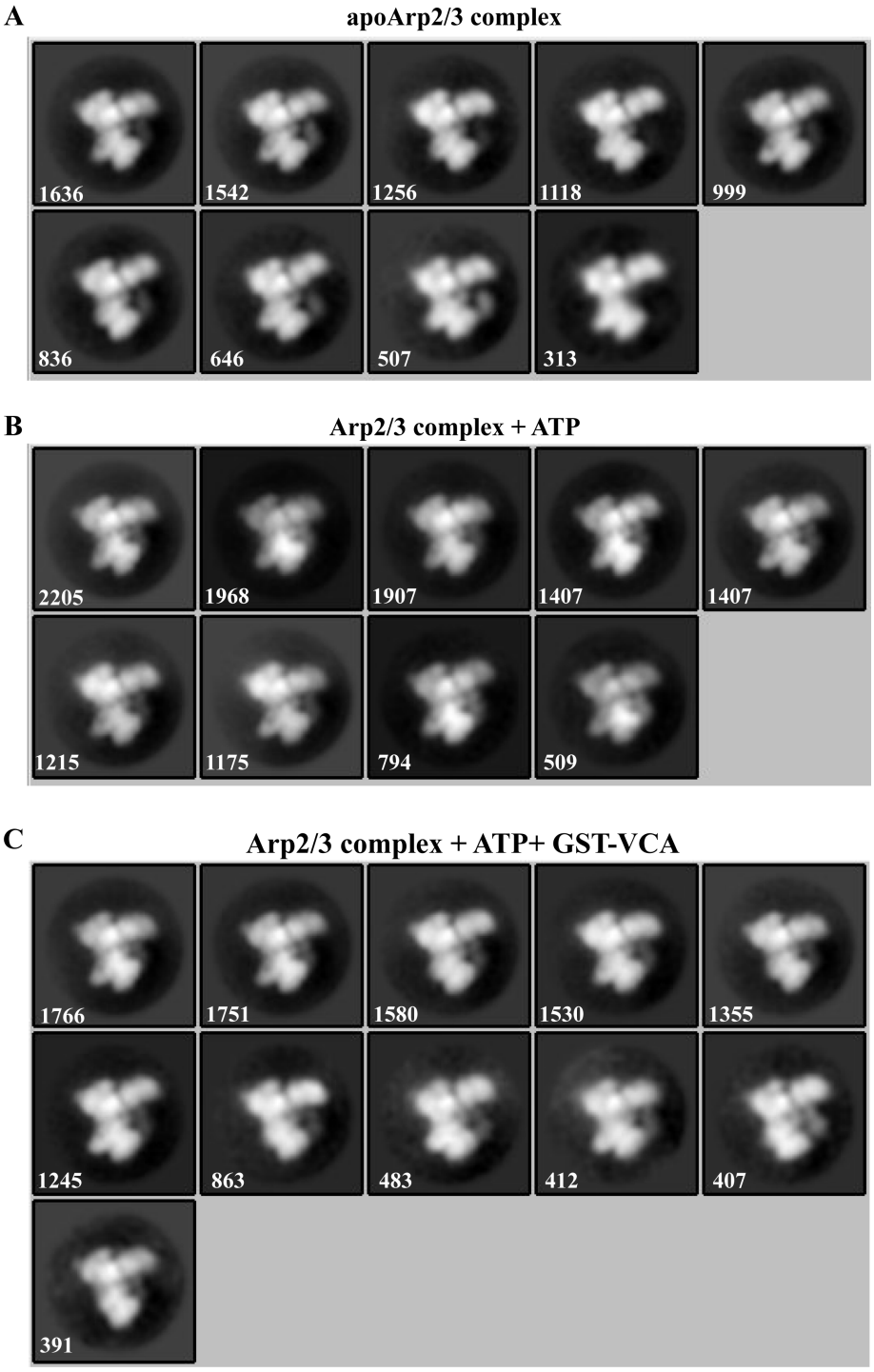

Figure S4. Class averages of electron micrographs of apo Arp2/3 complex alone, Arp2/3 complex bound to ATP and Arp2/3 complex with GST-VCA. Samples were prepared by negative staining and imaged by transmission electron microscopy. Numbers of particles in each class average are in white. All class averages are reported. (A) Electron micrographs of Arp2/3 complex treated with Dowex resin to remove ATP. (B) Arp2/3 complex in the presence of 0.2 mM ATP. (C) Arp2/3 complex in the presence of 0.2 mM ATP and 0.25 μM GST-VCA.

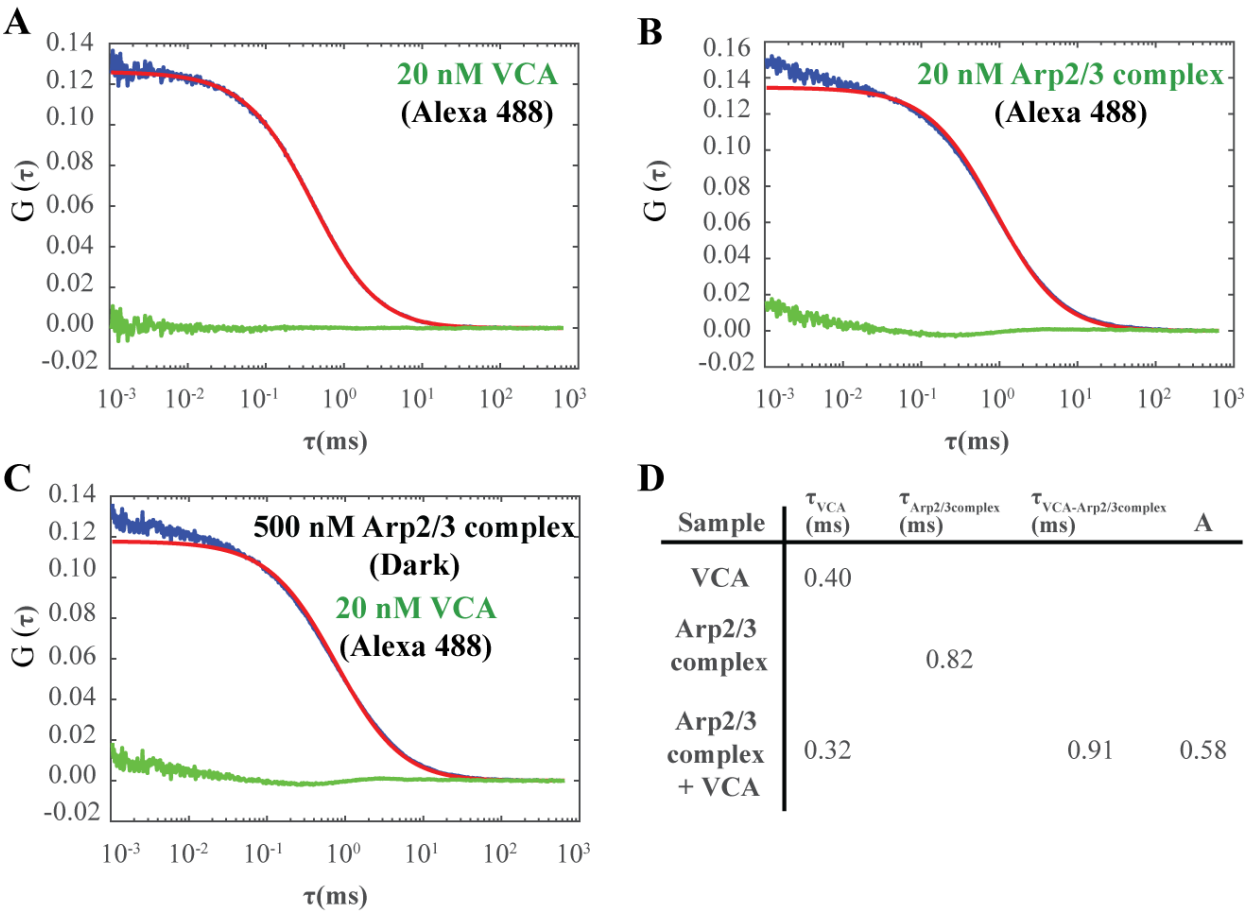

Sample	τ_{VCA} (ms)	$\tau_{Arp2/3complex}$ (ms)	$\tau_{VCA\text{-}Arp2/3complex}$ (ms)	A
VCA	0.40			
Arp2/3 complex		0.82		
Arp2/3 complex + VCA	0.32		0.91	0.58

Figure S5. Fluorescence Correlation Spectroscopy shows that VCA binds to Arp2/3 complex in our experimental conditions. Conditions: Room temperature in KMET buffer (50 mM KCl, 1 mM $MgCl_2$, 1 mM EGTA, 0.2 mM ATP, 1 mM DTT, 10 mM Tris-HCl, pH 7.0) (**A**) Blue: 20 nM VCA labeled on an N-terminal cysteine with Alexa 488. Green: Residuals (**B**) Blue: 20 nM Arp2/3 complex labeled with Alexa 488 on ArpC3. Green: Residuals (**C**) Blue: 20 nM VCA labeled with Alexa 488 with 500 nM unlabeled Arp2/3 complex. Green: Residuals (**D**) Diffusion times (τ) in ms for 20 nM Alexa 488-VCA, 20 nM Alexa 488-Arp2/3 complex, and 20 nM Alexa 488-VCA with 500 nM unlabeled Arp2/3 complex. Abundance (A) indicates the fraction of the $\tau_{Arp2/3complex\text{-}VCA}$ species in the sample. Deviation of the fit at fast time scales is due to the presence of free dye in the sample.

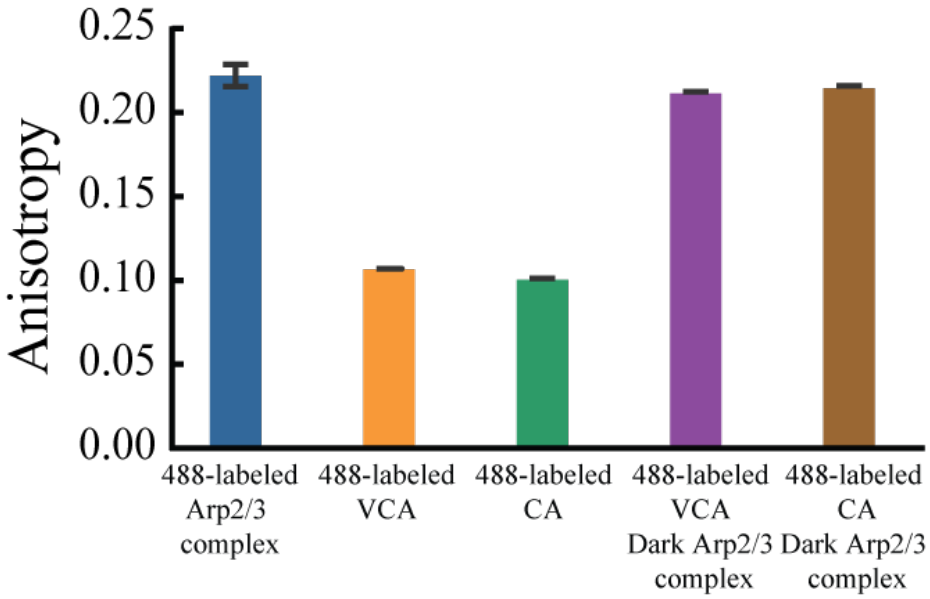

Figure S6. Fluorescence Anisotropy shows that VCA and CA bind Arp2/3 complex in our experimental conditions. Histogram with mean values and standard deviations from 4 measurements. Conditions: KMET buffer, 10 mM Tris-HCl, 50 mM KCl, 1 mM EGTA, 1 mM $MgCl_2$, 1 mM DTT, and 0.2 mM ATP. Samples: 100 nM Arp2/3 complex labeled on ArpC3 with Alexa 488; 50 nM Wsp1p-VCA and Wsp1-CA labeled on N-terminal cysteines with Alexa 488 alone or with 3 μM unlabeled Arp2/3 complex.

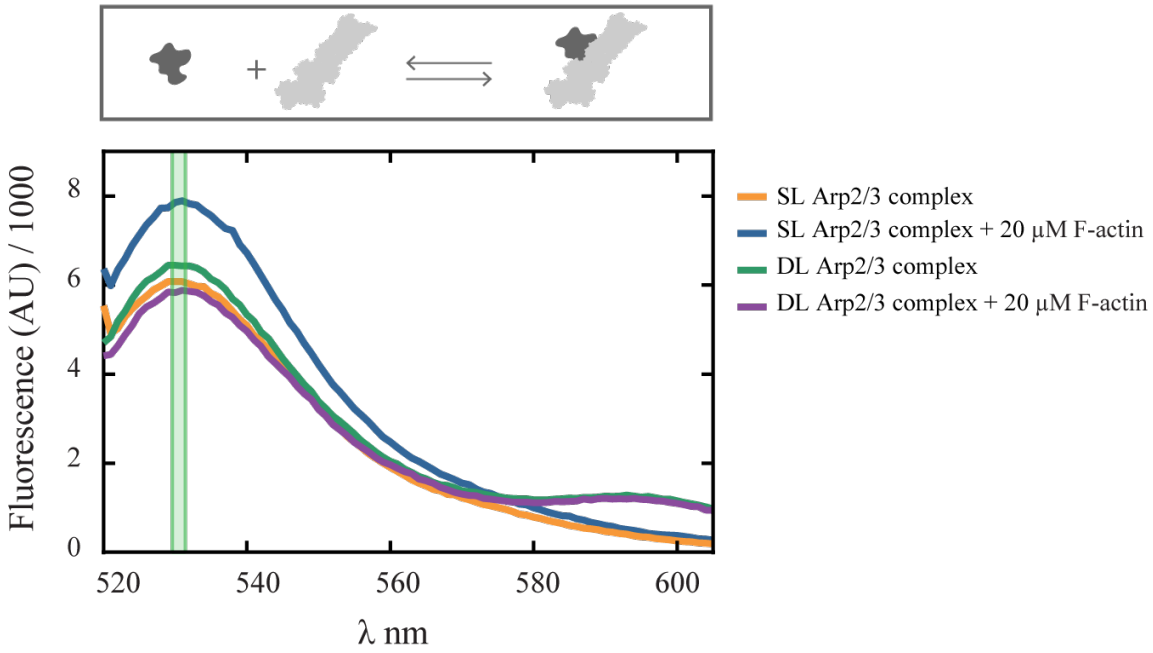

Figure S7. Measurement of FRET of bulk samples with fluorescence emission scans. All samples contained 20 nM Arp2/3 complex, either single-labeled (SL) on Arp2 with FlAsH-EDT_2 or double-labeled (DL) on Arp2 with FlAsH-EDT_2 and on Arp3 with Alexa 568, in KMEI buffer (10 mM imidazole, 50 mM KCl, 1 mM EGTA, 1 mM $MgCl_2$, 1 mM DTT, 0.2 mM ATP). Arp2/3 complex was incubated overnight (~12 h) with 20 µM polymerized actin. FlAsH-EDT_2 was excited at λ 510 nm and emitted light was collected with a wavelength scan from 520 nm to 610 nm. Ligands increased the donor (FlAsH EDT2) intensity of SL Arp2-Arp3 and ARPC1-ARPC3, suggesting that binding affected the local environment of the fluorophores. We assume that the ligands have same effect on the emission of FlAsH-EDT_2 on both single- and double-labeled complexes when calculating ET_{eff}. Energy transfer efficiencies were calculated using Equation S1 (Supplemental Materials and Methods). The fluorescence values used in this equation were the average fluorescence obtained from λ 530 nm to λ 532 nm (green bar) of single-labeled (for F_D) or double-labeled complexes (for F_{DA}). Figure 7 responds ΔET_{eff} values calculated by subtracting the ET_{eff} at 0 µM actin from the ET_{eff} at 20 µM actin. Reporting ΔET_{eff} allows us to compare the state of the complex with and without bound ligands.

Table S1 – Effects of ligands on energy transfer efficiency between probes on Arp2/3 complex measured by single molecule FRET and ALEX

		Energy Transfer Efficiency (ET_{eff})					***ALEX***				
Construct	***Ligand***	***Mean Peak***	***Mean Width ± SD***	***Minimum***	***Maximum***	***n***	***Mean Peak***	***Mean Width ± SD***	***Minimum***	***Maximum***	***n***
ArpC1-ArpC3	*None*	0.25	± 0.11	0.14	0.36	7	0.25	± 0.10	0.15	0.35	5
	VCA	0.28	± 0.13	0.16	0.41	4	0.30	± 0.10	0.19	0.39	1
	$Actin_{(m)}$-VCA	0.27	± 0.11	0.16	0.38	3	0.26	± 0.10	0.16	0.36	1
	CA	0.28	± 0.11	0.16	0.39	3	0.28	± 0.10	0.17	0.37	3
Arp3-Arp2	*None*	0.48	± 0.14	0.34	0.62	9	0.46	± 0.16	0.30	0.62	1
	VCA	0.61	± 0.09	0.52	0.70	4	0.62	± 0.10	0.52	0.72	1
	$Actin_{(m)}$-VCA	0.54	± 0.19	0.35	0.72	6	0.55	± 0.20	0.35	0.75	1
	CA	0.60	± 0.12	0.49	0.72	3	0.58	± 0.12	0.46	0.70	2

Mean values for the centers of the Gaussian distributions of FRET events and width calculations for a subset of measurements (n) on each sample obtained with smFRET and ALEX. Photon threshold was fixed at 30 for all calculations. Maximum and minimum ET_{eff} values were calculated by adding or subtracting the mean width value to the mean peak one. These numbers display the range of ET_{eff} values obtained. Measurements were made on 75 pM double-labeled Arp2/3 complexes ($Arp2_{cys}$-$Arp3_{cys}$ and $ArpC1_{cys}$-$ArpC3_{cys}$) in KMET buffer (10 mM Tris-HCl, 50 mM KCl, 1 mM EGTA, 1 mM $MgCl_2$, 1 mM DTT, and 0.2 mM ATP) alone or with 20 µM Wsp1p-VCA, 2 µM actin-Wsp1p-VCA or 20 µM Wsp1p-CA.

Table S2 – Effects of ligands on energy transfer efficiency between probes on Arp2/3 complex measured by ensemble FRET

	$Arp2_{tetracys}$-$Arp3_{cys}$			$ArpC3_{tetracys}$-$ArpC1_{cys}$		
Ligand	***Mean***	***Standard Deviation***	***n***	***Mean***	***Standard Deviation***	***n***
2mM ATP	0.01	± 0.02	4	-0.05	± 0.04	4
20 μM *CA*	0.12	± 0.02	3	-0.06	± 0.05	4
20 μM *VCA*	0.16	± 0.02	4	0.01	± 0.04	3
20 μM *GST-VCA*	0.16	± 0.04	4	-0.04	± 0.04	4
2 μM $Actin_{(m)}$-*VCA*	0.15	± 0.03	4	-0.05	± 0.02	3
10 μM *F actin-VCA*	0.22	± 0.03	3	0.22	± 0.02	3
20 μM *F actin*	0.26	± 0.02	3	0.16	± 0.02	4

Labeled constructs were diluted to fixed a concentration of 20 nM in KMEI buffer (10 mM imidazole, 50 mM KCl, 1 mM EGTA, 1 mM $MgCl_2$, 1 mM DTT). All samples had 0.2 mM ATP, except when testing the effect of ATP. For that experiment, ATP was either at 0 mM or 2 mM. Samples were incubated for 3 h at room temperature with a range of concentrations of VCA, CA, actin-VCA, GST-VCA, or a fixed concentration of polymerized actin and a range of concentrations of VCA. Complexes were incubated overnight (~12 h) with a range of concentrations of polymerized actin. Energy transfer efficiencies were obtained by comparing the donor intensities of double-labeled with single-labeled complexes (See supplemental methodology for details). Mean and standard deviations were calculated using different number of repetitions (*n*).

Table S3 – Fluorescence anisotropy values for single-labeled Arp2/3 complex

Alexa 488	***Average (n = 4)***	***Standard Deviation***
$ArpC1_{cys}$	*0.24*	*0.002*
$ArpC3_{cys}$	*0.22*	*0.002*
$Arp3_{cys}$	*0.22*	*0.001*
$Arp2_{cys}$	*0.21*	*0.001*

Alexa 594	***Average (n = 4)***	***Standard Deviation***
$ArpC1_{cys}$	*0.21*	*0.003*
$ArpC3_{cys}$	*0.21*	*0.004*
$Arp3_{cys}$	*0.22*	*0.001*
$Arp2_{cys}$	*0.23*	*0.002*

Arp2/3 complex was labeled on single site on four subunits (Arp2cys, Arp3cys, ArpC1cys, and ArpC3cys) Alexa 488 or Alexa 594. Samples were each diluted to 100 nM concentration in KMET buffer (10 mM Tris-HCl, 50 mM KCl, 1 mM EGTA, 1 mM $MgCl_2$, 1 mM DTT, and 0.2 mM ATP). Alexa 488 was excited at λ 490 nm and emitted light collected at λ 520 nm. Alexa 594 was excited at λ 590 nm and emitted light collected at λ 630 nm. Four measurements were performed per labeled construct.

Table S4 –Fluorescence lifetimes of single-labeled Arp2/3 complexes

Subunit	***T1 Component***
$ArpC1_{cys}$	*4.09 ns*
$ArpC3_{cys}$	*4.10 ns*
$Arp3_{cys}$	*4.10 ns*
$Arp2_{cys}$	*4.20 ns*
Free dye	*4.10 ns*

Arp2/3 complex with a single Alexa 488 label on one subunit (Arp2cys, Arp3cys, ArpC1cys, or ArpC3cys) was each diluted to 40 nM in KMET buffer (10 mM Tris-HCl, 50 mM KCl, 1 mM EGTA, 1 mM $MgCl_2$, 1 mM DTT, and 0.2 mM ATP). Samples were excited at 459 nm with a nano-LED and the emission at 517 nm was recorded. Fluorescence lifetime measurements confirm that quenching of the donor fluorophore does not affect the Förster radius under these conditions.

Table S5 – Sequences of primers used for C-terminal tagging of Arp2/3 complex subunits.

Construct	***Primer Name***	***Sequence 5' – 3' (Bahler, Wu et al. 1998)***
ArpC1$_{cys}$	*ArpC1cysFw*	GACCTTACGCTGGGACTCCTGGCAATATTACTGCGTTTACCTCCAGCGGTACCGACGG ACGTGTTGTTTTGTGGACTCTTTGTTAGCGGATCCCCGGGTTAATTAA
ArpC1$_{cys}$	*ArpC1cysRv*	GATTGTTCAATTCTTTTATTCTATGAGATTAACATCTACGGAAATTCGATAATTGATT TGATAAGATTCATTTGCCGATATCTTTTGAATTCGAGCTCGTTTAAAC
ArpC3$_{cys}$	*ArpC3cysFw*	ATGTATATGCAACTGAAAAGGATCATCCCAGCAAGTGGTGGACTTGCTTCAGCAAGAG ACGTTTTATGAACAAAGCTTTGTGTTAGCGGATCCCCGGGTTAATTAA
ArpC3$_{cys}$	*ArpC3cysRv*	GATTGTAAGCCGCATTTGAAATAAAGGAAACGGAAAAACATAAAGGCTTTGAAATACA GTATGAGCCAAATTATTAATTAATAGACGAATTCGAGCTCGTTTAAAC
Arp3$_{cys}$	*Arp3cysFw*	CCTATTGCCATACCAAAGCAGATTACGAAGAATATGGTGCTTCCATTGCTCGTAGGTA CCAAATTTTTGGAAATTCTCTTTGTTAGCGGATCCCCGGGTTAATTAA
Arp3$_{cys}$	*Arp3cysRv*	GATTGTTCTAAGGCTAATGCCTGCTCCATTAAACTTTTCATTTTAATCAGTAAATCCT ATAGACGCAAAACTCATGATATATTTCAGAATTCGAGCTCGTTTAAA
Arp2$_{cys}$	*Arp2cysFw*	ACGATCACATGTGGGTGTCCAAGGCAGAATGGGAGGAGTATGGAGTACGTGCACTAGA CAAATTGGGTCCTAGAACTACTTGTTAGCGGATCCCCGGGTTAATTAA
Arp2$_{cys}$	*Arp2cysRv*	GATTGTAATTTATGAATCAAACTTCGTATAACTCAATTTACTAGCACATAAAAAGAAA GAAACAGAACATTAAACATAAATATACTGAATTCGAGCTCGTTTAAAC
ArpC3$_{tetracys}$	*ArpC3tetracysFw*	ATGTATATGCAACTGAAAAGGATCATCCCAGCAAGTGGTGGACTTGCTTCAGCAAGAG ACGTTTTATGAACAAAGCTTTGTGTTGTTGTTGTTAGCGGATCCCCGGGTTAATTAA
ArpC3$_{tetracys}$	*ArpC3tetracysRv*	GATTGTTGTTGTTGTAAGCCGCATTTGAAATAAAGGAAACGGAAAAACATAAAGGCTT TGAAATACAGTATGAGCCAAATTATTAATTAATAGACGAATTCGAGCTCGTTTAAAC
Arp2$_{tetracys}$	*Arp2tetracysFw*	ACGATCACATGTGGGTGTCCAAGGCAGAATGGGAGGAGTATGGAGTACGTGCACTAGA CAAATTGGGTCCTAGAACTACTTGTTGTTGTTGTTAGCGGATCCCCGGGTTAATTAA
Arp2$_{tetracys}$	*Arp2tetracysRv*	GATTGTTGTTGTTGTAATTTATGAATCAAACTTCGTATAACTCAATTTACTAGCACAT AAAAAGAAAGAAACAGAACATTAAACATAAATATACTGAATTCGAGCTCGTTTAAAC
ArpC1$_{cys}$	*ArpC1cysFwChk*	ATTATCTCAATTGCCTTTGCGT
ArpC1$_{cys}$	*ArpC1cysRvChk*	CACTTCTCAATTTTGGGGTCTC
ArpC3$_{cys}$	*ArpC3cysFwChk*	TATCAGTGAGTGCTTGGGAAGA
ArpC3$_{cys}$	*ArpC3cysRvChk*	GAGGTTTTAAAGCACAATTCGG
Arp3$_{cys}$	*Arp3cysFwChk*	AAACATTGTCCTTTCTGGTGGT
Arp3$_{cys}$	*Arp3cysRvChk*	CTCAATGAAAAAGCCTGGAAAC
Arp2$_{cys}$	*Arp2cysFwChk*	GTGAACAACCAGGTTTGAGTGA
Arp2$_{cys}$	*Arp2cysRvChk*	ACGTCACGGGAGTCTAGTCATT

Primers for PCR-based gene targeting in *S. pombe* and checking primers were generated using the Bahler Lab web-interface script: *"PPPP: Pombe PCR Primer Program C-terminal tagging"*. (url: http://bahlerweb.cs.ucl.ac.uk/cgi-bin/PPPP/pppp_c_term.pl)

Supplemental Materials and methods

Cloning and mutation of S. pombe Arp2/3 complex

We added a single reactive cysteine to the C-termini of Arp2, Arp3, ArpC1 or ARPC3 or a peptide with four cysteines (CCCC) on the C-termini of ArpC3 or Arp2 by transforming a DNA fragment encoding the extra residues fused to a nourseothricin (NAT) selection marker into the G418-resistant C167S strain of *S. pombe* (1). The C167S *S. pombe* strain has the only reactive cysteine in native Arp2/3 complex replaced by serine (2). For double mutants, we crossed two different single mutant strains on SPA5 plates and separated the spores by tetrad dissection. After tetrad dissection, we grew the spores on YE5S agar plates at 25°C for 1 day and then replica-plated colonies onto YE5S-G418/NAT plates. PCR amplification and DNA sequencing confirmed strains with the desired mutations. Single and double mutants were compared with WT cells for growth at 23, 30 and 32°C. Supplemental Table S5 gives the sequences of the primers used for these steps.

Protein Purification and Labeling (Extended)

S. pombe Arp2/3 complex: We purified Arp2/3 complex from fission yeast by three chromatography steps: GST-VCA affinity column (GE Healthcare Life Sciences), ion exchange on a MonoQ 5/50 column (GE Healthcare Life Sciences), and size exclusion on a HiLoad Superdex 200 16/600 column (GE Healthcare Life Sciences) (3). We measured the concentration of the purified protein by absorption at 290 nm (ε = 139 030 M^{-1} cm^{-1}). Purity was verified by SDS-PAGE and staining with Coomassie blue (Figs. 2A and S4). After gel filtration, ArpC1cys-ArpC3cys and Arp2cys-Arp3cys constructs were exchanged by washing four times with 15 ml aliquots of low salt buffer (50 mM KCl, 10 mM imidazole, 1 mM $MgCl_2$, 1 mM EGTA, 0.1 mM ATP, pH 7) using a 30K Amicon Ultra centrifugal filter unit. We labeled mutant Arp2/3 complexes with Alexa-Fluor-488-C_5-maleimide (Alexa488) or/and Alexa-Fluor-594-C_5-maleimide (Alexa594) (ThermoFisher) in low salt buffer. For single mutants we used 10x molar excess of dye and for double mutants, 10x fold molar excess of acceptor (Alexa594) and 2x fold molar excess of donor (Alexa488). Incubating the protein for 2 min with 5x fold molar excess of 5,5-dithio-bis-(2-nitrobenzoic) acid (DTNB) before labeling with the dyes reduced unspecific labeling. Immediately after this pretreatment, the protein was transferred to a second microcentrifuge tube which contained the dye(s) and enough volume of high salt buffer (2 M KCl, 10 mM imidazole, 1 mM $MgCl_2$, 1 mM EGTA, 0.1 mM ATP, pH 7) to bring the salt

concentration up to 170 mM KCl. Proteins were incubated 45 min at 4°C and buffer was exchanged into low salt buffer with 1 mM DTT using a 30K Amicon Ultra centrifugal filter unit. After gel filtration, ArpC1cys-ArpC3tetracys and Arp3cys-Arp2tetracys constructs were buffer exchanged into FlAsH labeling buffer (170 mM KCl, 10 mM imidazole, 1 mM $MgCl_2$, 1 mM EGTA, 0.3 mM ATP, 0.1 mM BAL, pH 7) using a 30K Amicon Ultra centrifugal filter unit. We labeled both mutant Arp2/3 complexes overnight at 4°C with 10x molar excess 4,5-Bis(1,3,2-dithiarsolan-2-yl)-3,6-dihydroxyspiro[isobenzofuran-1(3H),9-[9H]xanthen]-3-one (FlAsH-EDT2) (Santa Cruz Biotechnology). Protein complexes were buffer exchanged into low salt buffer using a 30K Amicon Ultra centrifugal filter unit. Before labeling with 10x molar excess of Alexa 568 dye, complexes were incubated for 2 min in 5x fold molar excess of DTNB. Immediately after, the protein was transferred to a second microcentrifuge tube containing the dye and enough high salt buffer to raise the salt concentration to 170 mM KCl. Under these conditions, incubation with DTNB prevented Alexa 568 labeling the tetra cysteine peptide. Fig. 2A shows that Alexa 594 does not label the tetra cysteine tag. Proteins were incubated 45 min at 4°C and then exchanged into low salt buffer with 1 mM DTT using a 30K Amicon Ultra centrifugal filter unit. Remaining free dye was removed from all the four constructs using a 40K Zeba™ spin desalting column (ThermoFisher) equilibrated with low salt buffer with 1 mM DTT. Labeling efficiency was determined by absorption at λ 495 nm (ε 73,000 M^{-1} cm^{-1}) for Alexa 488, λ 594 nm (ε 92,000 M^{-1} cm^{-1}) for Alexa594, λ 538 nm (ε 70,000 M^{-1} cm^{-1}) for FlAsH-EDT2 (4), and λ 578 nm (ε 91,300 M^{-1} cm^{-1}) for Alexa586. Absorption values were corrected for dye absorption at λ 280 nm, λ 400 nm, and λ 495 nm or λ 594 nm when applicable. We used freshly made complexes for spectroscopic measurements.

VCA and CA constructs: We expressed *S. pombe* Wsp1p-VCA (497Q–574D), Wsp1p-VCAcys (496C–574D), and Wsp1-CA (541SC–574D) as GST fusions in plasmid pGV67 in Rosetta (DE3) pLysS *E. coli* cells (Novagen). We purified the proteins by DEAE anion exchange chromatography and glutathione Sepharose 4B affinity chromatography. Following cleavage of VCA/CA from GST by TEV protease, VCA and CA were separated from GST by ion exchange chromatography on a RESOURCE Q column (GE Healthcare Life Sciences) and size exclusion chromatography on a HiLoad Superdex 75 16/600 column (GE Healthcare Life Sciences). We measured concentrations of unlabeled VCA and CA by absorption at 280 nm (ε = 5690 M^{-1} cm^{-1}) (3) and verified purify by SDS-PAGE and staining with Coomassie blue (Fig. S4). We labeled a cysteine added to the N terminus of VCA and CA using a 10x molar excess of Alexa-

Fluor-488 C5-maleimide overnight at 4°C in labeling buffer (20 mM Tris-Cl, 100 mM NaCl, 1 mM EDTA, pH 8.0). Labeled constructs were separated from free dye by size exclusion on a HiLoad Superdex 75 16/600 column equilibrated with gel filtration buffer (20 mM Tris-Cl, 100 mM NaCl, 1 mM EDTA, 1 mM DTT, pH 8.0). Labeled constructs were used in fluorescence anisotropy and FCS experiments. Labeling efficiency was determined by absorption at 495 nm (ε 73 000 M^{-1} cm^{-1}). Absorption values were corrected for dye absorption at λ 280 nm and λ 400 nm.

Actin: We purified actin from chicken breast muscle acetone powder (5) by one cycle of polymerization and depolymerization followed by size exclusion chromatography on Sephacryl S-300 in G-buffer (2 mM Tris–HCl, 0.2 mM ATP, 0.1 mM $CaCl_2$ and 0.5 mM DTT, pH 8.0). The concentration of actin was measured by absorption at 290 nm (ε 26 600 M^{-1} cm^{-1}). Monomeric actin was polymerized in labeling buffer (50 mM PIPES, 50 mM KCl, 0.2 mM ATP, 0.2 mM $CaCl_2$, pH 7) and labeled on Cys374 with 7x molar excess of pyrene-iodoacetamide (6) or 10x molar excess Alexa-Fluor-488- C5-maleimeide (7) overnight at 4°C. Labeled actin was depolymerized using G-buffer, clarified and monomers were purified by size exclusion chromatography on Sephacryl S-300 in G-buffer. Purity was verified by Coomassie blue staining SDS-PAGE (Fig. S4). Labeling efficiency was determined by absorption at λ 344 nm (ε 22,000 M^{-1} cm^{-1}) for pyrene-iodoacetamide and at λ 495 nm (ε 73,000 M^{-1} cm^{-1}) for Alexa 488. Absorption values were corrected for dye absorption at λ 280 nm and λ 400 nm.

Accessible Volume (AV) calculation

We calculated Accessible Volumes (AV) for the conjugated dyes using the FPS software (8). Parameters used to generate AV clouds were length 20, width 4.5, and dye radius 3.5 Å for the donor fluorophore (Alexa 488) (8) and length 20, width 4.5, and dye radius 4 Å for the acceptor fluorophore (Alexa 594) (9). Inter-dye distances in these models were calculated using the AV mean fluorophore positions.

Crosslinking Actin to VCA

cys-VCA was dialyzed overnight against 2 L labeling buffer (2 mM Tris-Cl, 0.1 mM $CaCl_2$, 1 mM NaN_3, 0.1 mM ATP, 2 mM TCEP-HCl, pH 8). cys-VCA (25 μM) was incubated with 18.2 mM N,N′-m-phenylenedimaleimide (PDM) for 4 h at 4°C. Precipitated PDM was pelleted by centrifuging for 10 min at 2,500 g. The supernatant was dialyzed three times against 1 L of labeling buffer for 1 h at 4°C. Meanwhile, actin monomers were dialyzed against 1 L of labeling

buffer for 1 h at 4°C and then 2 L for 2 h. A 10x fold molar excess of PDM-cys-VCA was incubated with actin overnight at 4°C. Crosslinked products were purified by a three-step column purification: gel filtration on a HiLoad Superdex 75 16/60 column, ion exchange on a MonoQ 10/100 column, and a second round of size exclusion on a HiLoad Superdex 75 16/60 column (3). Purity was verified by SDS-PAGE and staining with Coomassie blue (Fig. S4).

Actin Polymerization Assays

We tested the functional integrity of our modified Arp2/3 complexes using pyrene actin polymerization assays (10). Reactions contained 3.5 μM actin monomers (10% pyrene-labeled), 50 nM Arp2/3 complex, 500 nM WASP–VCA in KMEI buffer (10 mM imidazole, 50 mM KCl, 1 mM EGTA, 1 mM $MgCl_2$, 1 mM DTT). Polymerization was monitored over time by fluorescence with excitation at λ 365 nm and emission at λ 407 nm using Spectramax Gemini XPS Microplate Spectrofluorimeter.

Ensemble FRET measurements (Extended)

Measurements were made in a PTI Alpha-scan fluorimeter (Photon Technology International) (11). FlAsH-EDT_2 single-labeled ($Arp2_{FlAsH}$ and $ArpC3_{FlAsH}$) and FlAsH-EDT_2 and Alexa 568 double-labeled complexes ($Arp2_{FlAsH}$-$Arp3_{Alexa568}$ and $ArpC3_{FlAsH}$-$ArpC1_{Alexa568}$) were diluted to fixed labeled concentrations of 20 nM in KMEI buffer. All experiments had 0.2 mM ATP present, except when testing the effect ATP on constructs where ATP was either at 0 mM or 2 mM. Complexes were incubated for 3 h at room temperature with a range of concentrations of VCA, CA, actin-VCA, GST-VCA, or a fixed concentration of polymerized actin with a titration of VCA. Complexes were incubated overnight (~12 h) with a range of concentrations of actin filaments). FlAsH-EDT_2 was excited at λ 510 nm and emitted light was collected with a wavelength scan from 520 nm to 650 nm. Changes in donor intensity of double-labeled complexes were calculated by comparing the average fluorescence obtained from λ 530 nm to λ 532 nm (emission peak) to single-labeled complexes.

Energy transfer efficiency, ET_{eff}, is defined as:

$$ET_{eff} = 1 - \frac{(F_D)}{(F_{DA})} \qquad \text{(Equation S1)}$$

where F_D is donor alone and F_{DA} is donor with the acceptor.

We recalculated energy transfer from the data of Goley et al. (12) using Equation S2:

$$ET_{eff} = \frac{(F_A)}{(F_{DA}+F_A)} \quad \text{(Equation S2)}$$

where F_A is emission of the acceptor alone and F_{DA} is the emission of the donor in the presence of the acceptor.

To transform distances (r) obtained from AV simulations to ET_{eff}s, ET_{eff} was defined as:

$$ET_{eff} = \frac{1}{1+(\frac{r}{R0})^6} \quad \text{(Equation S3)}$$

where r is distance and R_o is the Förster radius. R_0 for FRET pair Alexa 488/594 is 54 Å (13)

Total Internal Reflection Fluorescence (TIRF) Microscopy

We used a prism-style TIRF microscope to acquire fluorescence micrographs at 5 s intervals with a Hamamatsu C4747-95 CCD (Orca-ER) camera controlled by MetaMorph software (Molecular Devices) on an Olympus IX-70 inverted microscope (Olympus) (14, 15). Images were processed using ImageJ software (16).

Glass flow chambers (15) were incubated with 0.5% Tween 20, 250 nM *N*-ethylmaleimide-inactivated skeletal muscle myosin, and twice with 5% BSA (w/v), all in TBS_{HS} buffer (50 mM Tris-HCl, 600 mM KCl, pH 7.5) for 3 min each. Washes for 5 min with TBS_{HS} were made after each incubation step. Chambers were equilibrated with TIRF buffer (10 mM imidazole, 50 mM KCl, 1 mM $MgCl_2$, 1 mM EGTA, 50 mM DTT, 0.2 mM ATP, 0.2 µM $CaCl_2$, 15 mM glucose, 20 µg/ml catalase, 100 µg/ml glucose oxidase, and 0.5% methylcellulose (4,000 cP). 0.5 µM actin (30% labeled with Alexa 488) was polymerized in the chamber until short filaments were visible (2-5 min). Unpolymerized monomers were washed out and a mixture containing 100 nM Arp2/3 complex, 500 nM VCA, and fresh actin monomers was added during continuous imaging.

Negative Staining

Carbon-coated copper girds (Electron Microscopy Sciences, catalog No.: CF400-CU) were glow discharged using a homemade glow discharge unit (19). To absorb Arp2/3 complex to the glow discharged girds, 3.5 µL of 0.05 µM (0.011 mg/mL) Arp2/3 in KMEI buffer (50 mM KCl, 1 mM $MgCl_2$, 1 mM EGTA, 10 mM imidazole, pH 7.0), KMEI buffer with 0.2 mM ATP, or KMEI buffer with 0.2 mM ATP and 0.25 µM GST-VCA (*S. pombe* Wsp1p VCA, Q497-D574) was incubated on the grids at room temperature for 30 s. Grids were stained with three drops of freshly prepared 0.8% (w/v) uranyl formate, and dried in air.

Electron Microscopy

Specimens were inspected with a Tecnai F20 electron Microscope (FEI Company) operating at 200 kV. Images were recorded on a K2 Summit camera (Gatan Company) in counted mode at a nominal magnification of 29,000×, corresponding to a calibrated pixel size of 1.25 Å. The dose rate on the camera was set to ~8 counts/pixel/s, and the total exposure time was 12 s. Each image was fractionated into 20 frames (0.6 s/frame). The images were recorded at a defocus between -0.6 μm and -3.0 μm, and at a drifting speed of less than 0.2 nm/s.

2D Image processing

Dose-fractionated image stacks were motion-corrected and summed with MotionCorr (20). Summed images were binned by a factor of 2, resulting a pixel size of 2.5 Å. Particles were interactively picked using e2boxer in EMAN2/Sparx (21) using a box size of 120 pixels. Particle coordinates were exported from EMAN2 and imported into RELION2 (22) for 2D analysis. CTF estimation was performed using CTFFIND4 ((23)), and particles were CTF corrected before reference-free 2D classification with RELION2 and ISAC in EMAN2/Sparx (for the sample with GST-VCA only). For presentation purpose, the class averages were first sorted based on class distributions in RELION2, and then rotated to the same orientation using a cross-correlation-coefficient-based method, clipped to 100×100 pixels and masked with a radius of 40 pixels in EMAN2.

2D Projections

The Arp2/3 crystal structure (RCSB PDB: 4JD2) with visible Arp2 subdomains 1 and 2 (24) was used to generate 2D projections. Glial maturation factor (GMF) in the PDB file was manually removed before converting the atomic model to a density map. The map was centered in a cubic box (120 × 120 × 120 voxels; voxel size: 2.5 Å) and filtered at 20 Å. The 3D map was projected in various orientations to select a 2D projection similar to the EM 2D class averages. Command line programs in EMAN2 (21) were used for the conversation (e2pdb2mrc) and projection (e2project3d), which was rotated, clipped and masked like the EM 2D class averages.

Fluorescence Anisotropy

We performed anisotropy measurements to check rotational freedom of the fluorophores attached to our different constructs and to corroborate VCA and CA were bound properly to the different Arp2/3 complex constructs. Measurements were made in a PTI Alpha-scan

spectrofluorimeter (Photon Technology International, Santa Clara, California) (Marchand, Kaiser et al. 2001). For rotational freedom experiments, Arp2/3 complex labeled with Alexa 488 or Alexa 594 single subunits (Arp2cys, Arp3cys, ArpC1cys, and ArpC3cys) was diluted to 100 nM in KMET buffer (10 mM Tris-HCl pH 7.0, 50 mM KCl, 1 mM EGTA, 1 mM $MgCl_2$, 1 mM DTT, 0.2 mM ATP). Alexa 488 was excited at λ 490 nm and emitted light collected at λ 520 nm. Alexa 594 was excited at λ 590 nm and emitted light collected at λ 630 nm. Intensity scans at 1 s intervals were taken for 20 s, and the average anisotropy was calculated with PTI Felix Software. Fluorescence anisotropy, *r*, is defined as

$$r = \frac{(I_{VV} - G * I_{VH})}{(I_{VV} + 2G * I_{VH})} \qquad \text{(Equation S4)}$$

where I_{VV} and I_{VH} are the parallel and perpendicular components of the polarized fluorescence light, respectively. I_{VV} and I_{VH} were measured simultaneously using a T-shaped light path. G is a correction factor defined as $G = I_{HV}/I_{HH}$. To calculate *G*, solutions were excited with horizontally polarized light.

To verify VCA and CA binding to Arp2/3 complexes, we used Alexa 488 labeled VCA or CA at a fixed concentration of 50 nM and 3 μM unlabeled Arp2/3 complex in KMEI buffer. Measurements and calculations were performed as described above.

Fluorescence Lifetime Measurements

To confirm that the Förster radius was not altered by quenching of the donor fluorophore, we measured fluorescence lifetimes with a TCSPC TD-Fluor Horiba Fluorolog 3 Time Domain Fluorimeter. The samples were 40 nM Arp2/3 complex in KMET buffer with a single label on $Arp2_{cys}$, $Arp3_{cys}$, $ArpC1_{cys}$ or $ArpC3_{cys}$. We used a 459 nm nano-LED for excitation and 517 nm emission monochrometer. Slit widths were adjust to give an alpha measurement of 0.5 to 1.5% photon collection, and measurements continued until 10,000 photons were counted in the highest bin. All traces were fit to single-exponential and the T1 component is reported.

Fluorescence Correlation Spectroscopy (FCS)

FCS measurements were made on an inverted Olympus IX-71 microscope (Olympus) (17) using an adjusted laser power in the 4-6 μW range. Fluorescence emission was collected through the objective and filtered using a long-pass dichroic (Z488RDC) and a band-pass filter

(HQ600/200M- Chroma). Photons were passed through a 50-μm diameter optical fiber (OzOptics) directly coupled to an avalanche photodiode (Perkin-Elmer) (18). Experiments were done on passivated cover glasses with eight well chambers (Nunc). Each reaction contained 2 μM unlabeled Arp2/3 complex and/or 20 nM Alexa 488-labeled VCA.

Average autocorrelation curves were obtained by the averaging of thirty 15 s autocorrelation curves. In the cases of pure VCA or pure Arp2/3 complex, the autocorrelation curves were fit with a single component diffusion model, weighted by the inverse of the standard deviation (equation S2):

$$G(\tau) = \frac{1}{N}\frac{1}{1+\frac{\tau}{\tau_D}}\sqrt{\frac{1}{1+\frac{s^2\tau}{\tau_D}}} \qquad \text{(Equation S5)}$$

where, $G(\tau)$, is the autocorrelation value as a function of τ, τ_D is the average diffusion time of the particles, s is the ratio of the radial to axial dimension of the focal volume, and N is the average number of fluorescent particles in the focal volume.

After addition of unlabeled Arp2/3 complex to the labeled VCA, we observed two separate diffusing components in solution. The fast-diffusing species was fixed to the diffusion time of the VCA; the slower-diffusing species was allowed to float up to 0.2 ms above the Arp23 diffusion time to accommodate potential changes in hydrodynamic radius of the complex. The curves were fit with a two-component diffusion model (equation S6):

$$G(\tau) = \frac{1}{N}\left(A\frac{1}{1+\frac{\tau}{\tau_{d1}}}\sqrt{\frac{1}{1+\frac{s^2\tau}{\tau_{d1}}}} + (1-A)\frac{1}{1+\frac{\tau}{\tau_{d2}}}\sqrt{\frac{1}{1+\frac{s^2\tau}{\tau_{d2}}}}\right) \qquad \text{(Equation S6)}$$

where all components are as in Equation S5, but with the addition of A for the fractional percentage of component 1, and two diffusing species with diffusion times of τ_{d1} and τ_{d2}.

In addition to diffusing VCA and VCA/Arp2/3 complex, the sample contained a small amount of freely diffusing fluorophore. We judged that including a third diffusing component during fitting would produce a less accurate fit than by excluding it, so the fit at fast timescales (0.09 ms) deviated from the data.

References

1. Bahler J*, et al.* (1998) Heterologous modules for efficient and versatile PCR-based gene targeting in Schizosaccharomyces pombe. *Yeast* 14(10):943-951.
2. Beltzner CC & Pollard TD (2008) Pathway of actin filament branch formation by Arp2/3 complex. *J Biol Chem* 283(11):7135-7144.
3. Ti SC, Jurgenson CT, Nolen BJ, & Pollard TD (2011) Structural and biochemical characterization of two binding sites for nucleation-promoting factor WASp-VCA on Arp2/3 complex. *Proc Natl Acad Sci U S A* 108(33):E463-471.
4. Granier S*, et al.* (2007) Structure and conformational changes in the C-terminal domain of the beta2-adrenoceptor: insights from fluorescence resonance energy transfer studies. *J Biol Chem* 282(18):13895-13905.
5. MacLean-Fletcher S & Pollard TD (1980) Identification of a factor in conventional muscle actin preparations which inhibits actin filament self-association. *Biochem Biophys Res Commun* 96(1):18-27.
6. Pollard TD (1984) Polymerization of ADP-actin. *J Cell Biol* 99(3):769-777.
7. Mahaffy RE & Pollard TD (2006) Kinetics of the formation and dissociation of actin filament branches mediated by Arp2/3 complex. *Biophys J* 91(9):3519-3528.
8. Kalinin S*, et al.* (2012) A toolkit and benchmark study for FRET-restrained high-precision structural modeling. *Nat Methods* 9(12):1218-1225.
9. Metskas LA & Rhoades E (2015) Conformation and Dynamics of the Troponin I C-Terminal Domain: Combining Single-Molecule and Computational Approaches for a Disordered Protein Region. *J Am Chem Soc* 137(37):11962-11969.
10. Cooper JA, Walker SB, & Pollard TD (1983) Pyrene actin: documentation of the validity of a sensitive assay for actin polymerization. *J Muscle Res Cell Motil* 4(2):253-262.
11. Marchand JB, Kaiser DA, Pollard TD, & Higgs HN (2001) Interaction of WASP/Scar proteins with actin and vertebrate Arp2/3 complex. *Nat Cell Biol* 3(1):76-82.
12. Goley ED, Rodenbusch SE, Martin AC, & Welch MD (2004) Critical conformational changes in the Arp2/3 complex are induced by nucleotide and nucleation promoting factor. *Mol Cell* 16(2):269-279.
13. Schuler B, Lipman EA, & Eaton WA (2002) Probing the free-energy surface for protein folding with single-molecule fluorescence spectroscopy. *Nature* 419(6908):743-747.
14. Kuhn JR & Pollard TD (2005) Real-time measurements of actin filament polymerization by total internal reflection fluorescence microscopy. *Biophys J* 88(2):1387-1402.
15. Amann KJ & Pollard TD (2001) Direct real-time observation of actin filament branching mediated by Arp2/3 complex using total internal reflection fluorescence microscopy. *Proc Natl Acad Sci U S A* 98(26):15009-15013.
16. Schneider CA, Rasband WS, & Eliceiri KW (2012) NIH Image to ImageJ: 25 years of image analysis. *Nat Methods* 9(7):671-675.
17. Trexler AJ & Rhoades E (2009) Alpha-synuclein binds large unilamellar vesicles as an extended helix. *Biochemistry* 48(11):2304-2306.

18. Middleton ER & Rhoades E (2010) Effects of curvature and composition on alpha-synuclein binding to lipid vesicles. *Biophys J* 99(7):2279-2288.

19. Aebi U & Pollard TD (1987) A glow discharge unit to render electron microscope grids and other surfaces hydrophilic. *J Electron Microsc Tech* 7(1):29-33.

20. Li X, *et al.* (2013) Electron counting and beam-induced motion correction enable near-atomic-resolution single-particle cryo-EM. *Nat Methods* 10(6):584-590.

21. Tang G, *et al.* (2007) EMAN2: an extensible image processing suite for electron microscopy. *J Struct Biol* 157(1):38-46.

22. Scheres SH (2012) RELION: implementation of a Bayesian approach to cryo-EM structure determination. *J Struct Biol* 180(3):519-530.

23. Rohou A & Grigorieff N (2015) CTFFIND4: Fast and accurate defocus estimation from electron micrographs. *J Struct Biol* 192(2):216-221.

24. Luan Q & Nolen BJ (2013) Structural basis for regulation of Arp2/3 complex by GMF. *Nat Struct Mol Biol* 20(9):1062-1068.